Escola de Camins
Escola Tècnica Superior d'Enginyeria de Camins, Canals i Ports
UPC BARCELONATECH

TESI DE MÀSTER

Màster

Numerical Methods in Engineering

Títol

Model Order Reduction for hydraulic fracturing problems

Autor

Martí Burcet Rodríguez

Tutor

Sergio Zlotnik Martínez

Intensificació

30 ECTS

Data

22/09/2017

MODEL ORDER REDUCTION
FOR HYDRAULIC
FRACTURING PROBLEMS

by

Martí Burcet Rodríguez

in partial fulfillment of the requirements for the degree of

Master of Science
in Numerical Methods in Engineering

at the ETSECCPB, Universitat Politècnica de Catalunya.

Supervisor: Prof. Dr. S. Zlotnik Martínez

CONTENTS

1

INTRODUCTION

Hydraulic Fracturing is a technique used in the oil and gas industry since the decade of 1930's to increase well performance. It is of special interest to extract a type of non-conventional oil called *shale oil* from the subsurface. Shales are a type of rock with the particularity of extremely low permeabilities (in the order of $1 \times 10^{-6} - 1 \times 10^{-9}$ Darcy) although they may have much porosity than sandstones (in the order of 30%). This huge difference between high porosities and low permeabilities is a consequence of the tiny grain size. Standard reservoirs have porosities in the order of $1 \times 10^{-2} - 1 \times 10^{-1}$ Darcy. Therefore they may be an excellent reservoir rock although the natural extraction of oil or gas may be difficult.

Shale oil reservoirs are less profitable than standard ones but in the last decades with the increase in the oil price and new technologies have increased its profit. Two main discoveries have came to change this situation:

1. **Horizontal Drilling:** the possibility of drill horizontal wells instead of only vertical ones allows to increase the area of exposition which increases the extraction rate in low permeabilities rocks.

2. **Advances in Hydraulic Fracturing:** the idea of Hydraulic Fracturing is to artificially fracture the rock to increment the permeability.

The process of trigger artificial fractures in the rock consists in injecting a high pressure mixture of hydraulic fluids and sorted sand (proppant) [1]. The fracturing fluid when starts flowing through the rock develops a net of fractures around the borehole. Then once the injection stops, the induced fractures remain opened due to the proppant transported in the fracturing fluid. The final step is the pump exploitation that applies a negative gradient of pressure in the reservoir and the oil flows to the extraction pump.

Although hydraulic fracturing was first used in the hydrocarbon industry, it is also applied in other fields such that ground reinforcement, in petroleum engineering for reinjection of drilling cuttings or in environmental engineering for solids waste disposal [2].

However this process of injecting high pressure fluids into the rock may be sometimes dangerous in terms of environmental impact (groundwater pollution, vibrations, affection to biodiversity...) or even geotechnical risks (induced earthquakes, collapse...) [3]. This is because the pressure at which fluid has to be injected (wellbore pressure), usually the only control parameter during the operation, or the time it should last for is unknown at the time of injection. To improve this performance and to avoid risks, numerical simulations have been proposed and used since 1950's to study the evolution of hydraulic fractures in shale reservoirs [4].

Full numerical simulations is a costly process because of the domain size and because it's time dependent. In addition since the properties and geometry of the rock are in many cases quite uncertain (due to few geological tests or because their confidence level is low) the pre-well performance simulations may be inaccurate or even useless. Studies have shown that net-pressures found in the field can be up to 50 to 100 % higher than the ones predicted by conventional hydraulic fracturing simulators, and even more in weak formations [5]. Therefore it is necessary to found methods to fast integrate field data to update models and

increase their reliability.

The aim of this Master's Thesis is to check the suitability of a Model Order Reduction of the hydraulic fracturing problem. The final objective of the use of reduced order models in this kind of problem would be to run real-time simulations able to reintegrate in-situ data that could help in the optimal and safety completion of hydraulic fracturing processes.

1.1. HYDRAULIC FRACTURING MODELS

Several models have been developed over the years to study the development of hydraulic fractures in a solid media. This is a complex problem even for simplified problems because it may account for:

1. **Deformation of the rock**: normally modeled under Theory of Linear Elasticity.

2. **Fluid flow in the fracture**: under Lubrication Theory.

3. **Fracture propagation**: with the criterion of energy-release defined by the Stress Intensity Factor (SIF).

Different models have been developed to account for several macro-scale fracture shapes. The Perkins, Kern and Nordgen (PKN) model [6] is applicable to long fractures of limited height and elliptical cross-section (Figure 1.1a). On the other hand the Khristinaovic-Geertsma-de Klerk (KGD) model [7] is height independent and used in short fractures where horizontal plane-strain assumption is valid (Figure 1.1b). Finally the radial or penny-shaped model was solved by Sneddon [8] is valid in homogeneous reservoirs and the injection region is almost a point source (Figure 1.1c).
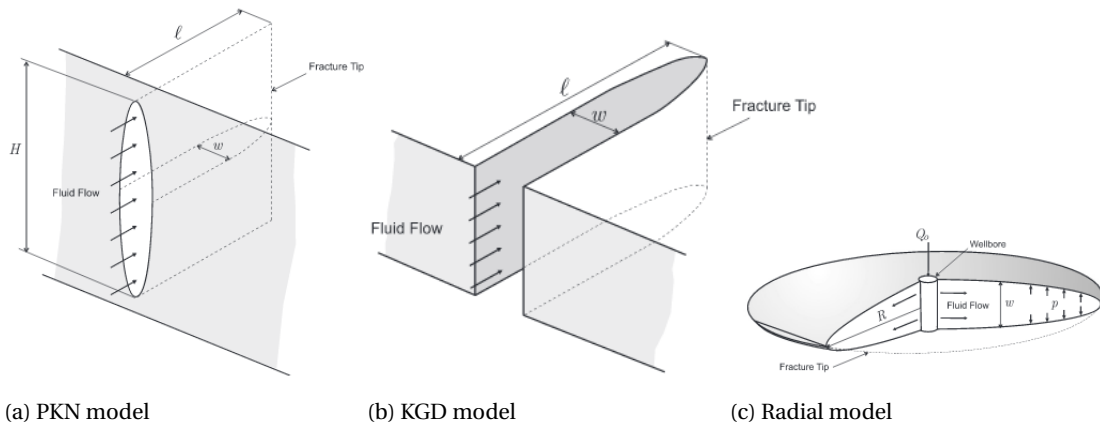

| (a) PKN model | (b) KGD model | (c) Radial model |

Figure 1.1: Squemes of three different fracture models [4].

Many modifications and updates have been proposed to these three models since they were first published to account for material toughness or power law fluids. However these models are not useful to treat multilayer reservoirs because the confining stress jump from one layer to the next one may be significant.

A first attempt to model fractures in different layers were the Pseudo-3D (P3D) models which are based on the assumption that elastic properties of the reservoir are homogeneous and averaged in the layers cut by the fracture. This assumption is yet valid because confining stress dominates elastic properties in the computation of fracture width.

A new branch of models arose under the general naming of Planar 3D (PL3D) models which uses a 2D mesh (either fixed or moving) to model the fracture footprint and the coupled fluid flow. Then the full 3D elastic equations are used to describe fracture width as a function of the fluid pressure.

Finally the most recent work has been devoted to develop full 3D models that, even though the access to many computational resources, have had limited success.

1.2. MODEL ORDER REDUCTION

The concept of Model Order Reduction was first introduced in the frame of theory of systems and control, where the aim was in reducing the complexity of dynamical systems while preserving input-output behaviors [9]. In numerical modeling the concept Model Order Reduction won importance specially after the publication of several methods such the Padé Via Lanczos (PVL) [10].

The basic idea of Model Order Reduction in numerical modeling is to simplify models containing many degrees of freedom to reduced ones that also produce reliable outcomes with treatable times and storage capacity. In the limit case, it is possible to run on-line simulations. These fast simulations are specially useful in optimization or inverse problems.

The principle of Reduced Order Models (ROM) techniques consists in capturing the essential features of the process we want to simulate in the early stage. In this way it is possible to represent an approximation of the general behavior of our model with fewer information than those of the full simulation. The way to extract relevant information from the system and the convergence criteria depend on the particular method applied.

The firsts approaches to Model Order Reduction came to light in 1980's and 1990's. In 1981 the Truncated Balanced Residual method was published by Moore. Then in 1984 Glover present the Hankel-norm reduction method. It was in 1987 when Sirovich proposed the Proper Orthogonal Decomposition (POD). A first method related to Krylov subspaces was published in 1990 (Asymptotic Waveform Evaluation) that was more centered in getting Padé approximations than finding Krylov spaces. In 1993 the relation between Padé approxiamtions and Krylov spaces was shown by Freun and Feldmann in the Padé Via Lanczos (PVL) method.

In the last two decades many other Model Order Reduction methods have arose to solve specific situations or more general cases. One of special interest for us is the Proper Generalized Method (PGD), first introduced in the context of computational rheology [11][12].

A distinction between ROM's is done based on if they can be computed directly, the so-called *a priori*, or if they first need a set of *snapshots* of the solution solved with another numerical method to extract from it relevant information. This second group of methods are called *a posteriori*. In the present thesis we compare the POD which is an *a posteriori* method with the PGD that is an *a priori* one. In the following sections we introduce the two methods.

1.2.1. PROPER ORTHOGONAL DECOMPOSITION

The objective of the Proper Orthogonal Decomposition is to obtain a proper orthonormal basis of rank l for the *snapshot set* of the solution of a problem given by n vectors (*snapshots*) $y_i, \ldots, y_n \in \mathbb{R}^m$, m being in the discrete case the number of nodes of our discretization. Since we are seeking for a model order reduction, $l \leq \min\{m, n\}$ is satisfied.

The POD is formulated as a constrained optimization problem, and the first-order optimality conditions are strongly related to the Singular Value Decomposition (SVD) of the rectangular matrix ($Y \in \mathbb{R}^{m \times n}$) containing per columns the *snapshots*. The rank of $Y = d \leq \min\{m, n\}$.

The SVD of a matrix Y gives as a result the decomposition in three matrices: Ψ, Y and Φ that satisfy the relation:

$$\Psi^T \cdot Y \cdot \Phi = \begin{pmatrix} D & 0 \\ 0 & 0 \end{pmatrix} := S \in \mathbb{R}^{m \times n} \tag{1.1}$$

where $D = diag(\sigma_1, \ldots, \sigma_d) \in \mathbb{R}^{d \times d}$ and the 0 matrices are of appropriate dimensions. The vectors $\{\Psi_i\}_{i=1}^d$ stored in the columns of Ψ and the vectors $\{\Phi_i\}_{i=1}^d$ stored in the columns of Φ satisfy

$$Y\phi_i = \sigma_i \psi_i \quad \text{and} \quad Y^T \psi_i = \sigma_i \phi_i \quad \text{for} \quad i = 1, \ldots, d \tag{1.2}$$

and represent the eigenvectors of the matrices YY^T and Y^TY respectively with associated eigenvalues $\lambda_i = \sigma_i^2 > 0$, $i = 1, \ldots, d$; and the set of eigenvectors $\{\Psi_i\}_{i=d+1}^m$ and $\{\Phi_i\}_{i=d+1}^n$ have zero as eigenvalues.

Once defined the matrices Ψ, S and Φ the following relation holds:

$$Y = \Psi \cdot S \cdot \Phi^T = \Psi^d \cdot D \cdot (\Phi^d)^T \tag{1.3}$$

where $\Psi^d \in \mathbb{R}^{m \times d}$ are the firsts d eigenvectors of Ψ and $\Phi^d \in \mathbb{R}^{n \times d}$ are the firsts d eigenvectors of Φ. In this way only the *relevant* eigenvectors, those with non-null amplitude, are stored [13].

The S matrix have the following properties [14]:

- **Pseudo-diagonality**: the only non zero elements of the matrix are those in the main diagonal of the rectangular matrix.

$$S = diag(\sigma_1, \sigma_2, \ldots, \sigma_d) \tag{1.4}$$

- **Ordering**: the amplitude of the diagonal components decreases.

$$\sigma_1 \geq \sigma_2 \geq \ldots \geq \sigma_{min} \geq 0 \tag{1.5}$$

Thanks to properties (1.4) and (1.5) it is possible to approximate Y with only a subset of the firsts eigenvectors $e < d$, those with bigger amplitudes σ_i because they contain most of the relevant information. This representation with less *modes* justifies the Model Order Reduction because allows recover the solution with savings in memory resources and in the computation time.

The fact that to get the separable representation with POD we need previously to compute the solution justifies classifying this method as an *a posteriori* one.

1.2.2. PROPER GENERALIZED DECOMPOSITION

The Proper Generalized Decomposition (PGD) is a reduced order technique applied in two phases: first an off-line process allows computing a base of elements, the *computational vademecum*, that in the second phase permit perform multiple on-line queries consisting on vector-vector products to recover the solution of the model with real-time response [15].

The fact that the solution of the model is directly constructed from the *computational vademecum* and not from a previously computed discrete solution classifies this method within the *a priori* ROM. This property makes of PGD not only a ROM technique but also an efficient solver for multidimensional models with many degrees of freedom that may lead to problems with the *curse of dimensionality*.

The *curse of dimensionality* is the name given to the problem caused by the exponential growth of volume associated with adding extra dimensions to Euclidean spaces. An illustrative example of this problem would be that a 1D mesh of a unit interval with size 1×10^{-2} needs 1×10^2 elements, while to keep the same mesh size for a 10D case, one would need 1×10^{20} elements [16]. Therefore even for a quite coarse mesh in a multidimensional problem, standard numerical methods become too costly and PGD is a powerful tool to solve it.

The basic idea of PGD is, given a D-dimensional problem, each dimension accounting for instance for physical entities, boundary conditions, material parameters... write a separable solution as a sum of N products of D functions $F_i^j(x_j)$ depending each one in only one variable. Both the number of terms of the summation N and the functions $F_i^j(x_j)$ are unknown *a priori* and determined during an iteratively enrichment process:

$$u^N(x_1, \ldots, x_D) = \sum_{i=1}^N F_i^1(x_1) \times \cdots \times F_i^D(x_D) \quad \text{in} \quad (x_1, \ldots, x_D) \in \Omega_1 \times \cdots \times \Omega_D \tag{1.6}$$

The computation of the functionals $F_i^j(x_j)$ is done invoking the weak form of the problem and integrating separately for each dimension. This is possible because at the enrichment step $n + 1$ all previous functions $F_i^j(x_j)$ are known for $i \leq n$. Therefore when aiming to compute $F_{n+1}^k \in \Omega_j$ all the rest of functions F_n^j for $j \neq k$ are known, so they can be moved to the right hand side. In this way at each enrichment step a system of one-dimensional non-linear equations is defined that has to be solved iteratively [17].

As said before the number of terms N of the summation is unknown and numerical experiment show that they don't depend on the problem dimension D but on the separable character of the solution. The stopping criteria for adding more modes is based in many cases on convergence of the solution $\|u^N - u^{N-1}\| \leq tol$.

The reduction in the number of unknowns is clear: if for example M nodes are used to discretize each dimension, the original problem had M^D unknowns defined in the cross product space $\Omega_1 \times \cdots \times \Omega_D$, while the PGD problem has $M \times N \times D$ unknowns to seek in the space $\sum_i^D \Omega_i$. Therefore the exponential growth in degrees of freedom with the dimensions of the problem has been stopped, or what is the same, the *curse of dimensionality* has been precluded.

2

FORMULATION

The hydraulic fracturing model is a complex problem because it is coupled and non-linear. The coupling comes from the fluid-solid interaction in the fracture because the tractions of the solid affects the fluid flow and vice-versa.

In a high compressed rock formation, as it is the case of a shale oil reservoir at great depth, the minimum in-situ stress is in the horizontal plane. Therefore the most usual hydraulic fractures develop in vertical planes perpendicular to the minimum stress [18]. The model chosen in this thesis is the Khristinaovic-Geertsma-de Klerk (KGD) that assumes a vertical hydraulic fracture of independent high growing radially to the fluid source under plane-strain conditions (see Figure 1.1b).

The KGD model studies a cross section of the vertical fracture and makes some assumptions to simplify it and keep the problem treatable, these assumptions are [7]:

1. **Homogeneous and isotropic solid**

2. Solid deformation is modeled under **linear elasticity theory**

3. Fracturing fluid flow behaves as **purely viscous**

4. Fluid flow inside the fracture is everywhere **laminar**

5. Fracture propagation (when considered) is assumed to **grow radially symmetrical from a point source**

The micro-scale classical geometry of the fracture front considers a void zone between the fracturing fluid front and the crack tip known as fluid lag, as it is shown in Figure 2.1.

In our model we have done some extra considerations to simplify the equations because our objective is to check the suitability of ROM in this problem more than apply complex models. This additional simplifications are:

6. There is **no fluid lag** zone

7. There is **no fluid leakage** neither from the fracturing fluid to the reservoir nor from the reservoir to the fracture

These two last consideration implies that the injected fracturing fluid occupies all the fracture.
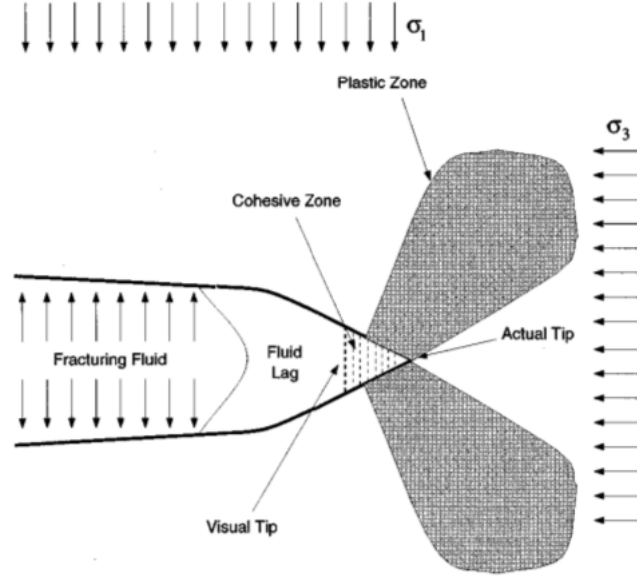
Figure 2.1: Classical geometry of a hydraulic fracturing front [2].

2.1. GOVERNING EQUATIONS

In the following sections we present the equations of the fracking fluid flow, for the reservoir solid deformation and for the advance criterion.

2.1.1. FLUID EQUATION

The fluid flow is modeled as a laminar flow between two parallel plates, defined as Poiseuille flow [19]. This equation relates the fracture opening rate with the fluid friction in the fracture and the inflow rate (2.1a):

$$\frac{\partial w}{\partial t} = \frac{\partial}{\partial s}\left(\frac{w^3}{12\mu}\frac{\partial p}{\partial s}\right) + \delta(s)Q_0 \tag{2.1a}$$

$$\delta(s) = \begin{cases} 0 & \text{if} \quad s > r \\ 1 & \text{if} \quad s \le r \end{cases} \tag{2.1b}$$

where w is the fracture opening, p is the pressure, s is the position inside the fracture, μ is the fluid viscosity, $\delta(s)$ is the Dirac's delta that only takes values at points placed inside the injection pipe of radius r and Q_0 is the inflow rate. Note the non-linear character of the equation due to the cubic term w^3.

This Initial Value Problem needs of an initial condition on pressure inside the fracture to proceed. This pressure cannot be arbitrary chosen because has to be in equilibrium with the confining stresses surrounding the initial fracture length. An initial pressure not in equilibrium may trigger numerical problems that can result in senseless solutions like negative pressures.

A method for computing a valid initial condition for pressure ($\hat{p}$) in a half domain is found solving the non-linear scalar equation (2.2) [20].

$$\hat{q}^*\left(\frac{w_0^\sigma}{w_0^*} + \frac{\hat{p}}{\hat{p}^*}\right)^3\left(\frac{\hat{p}}{\hat{p}^*}\right) - \frac{1}{2}Q_0 = 0 \tag{2.2a}$$

$$\hat{q}^* = \frac{1}{12\mu}(w_0^*)^3\frac{\hat{p}^*}{L_0} \tag{2.2b}$$

where w_0^σ is the initial fracture opening due to solely far field stress, w_0^* is the fracture opening at $t = 0$ resultant of applying an arbitrary pressure without far-field stress, $\hat{p}^*$ is an initial fracture pressure and L_0 is the initial fracture length. In our case we have considered that the fracture opening due to only far field stress

is $w_0^\sigma = 0$.

A good initial guess to start the iterative solver is proven to be (2.3) [20].

$$\hat{p} = \hat{p}^* \left(\frac{\frac{1}{2} Q_0}{\hat{q}^*} \right)^{1/4} \tag{2.3}$$

2.1.2. SOLID EQUATIONS

The equations of the solid are the ones of linear elasticity, that expressed in conservative form are:

$$\nabla \cdot \boldsymbol{\sigma}_e = \nabla \cdot (\mathbb{C} : \boldsymbol{\varepsilon}) = \nabla \cdot (\mathbb{C} : \nabla^s \boldsymbol{u}) = 0 \text{ in } \Omega \tag{2.4}$$

where $\boldsymbol{\sigma}_e$ is the effective stress tensor ($\boldsymbol{\sigma}_e = \boldsymbol{\sigma} - p_p$), p_p is the pore pressure $\boldsymbol{\varepsilon}$ is the strain tensor and $\mathbb{C}$ is the fourth-order elastic constitutive tensor, defined as:

$$\mathbb{C}_{ijkl} = \frac{\nu E}{(1+\nu)(1-2\nu)} \delta_{ij} \delta_{kl} + \frac{E}{2(1+\nu)} (\delta_{ik}\delta_{jl} + \delta_{il}\delta_{jk}) \tag{2.5}$$

where E is the Young's modulus, ν the Poisson's ratio and δ_{ij} is the Kronecker delta.

We consider a 2D plane-strain model (KGD) and therefore the equations can be simplified adopting engineering Voigt's notation as:

$$\nabla \cdot \boldsymbol{\sigma}_e = \nabla \cdot (\boldsymbol{D}\boldsymbol{\varepsilon}) = \nabla \cdot (\boldsymbol{D}\nabla^s \boldsymbol{u}) = 0 \text{ in } \Omega \tag{2.6}$$

where

$$\boldsymbol{D} = \frac{E(1-\nu)}{(1+\nu)(1-2\nu)} \begin{pmatrix} 1 & \frac{\nu}{1-\nu} & 0 \\ \frac{\nu}{1-\nu} & 1 & 0 \\ 0 & 0 & \frac{1-2\nu}{2(1-\nu)} \end{pmatrix}; \qquad \boldsymbol{\varepsilon} = \begin{pmatrix} \varepsilon_x \\ \varepsilon_y \\ \gamma_{xy} \end{pmatrix}; \qquad \boldsymbol{\sigma}_e = \begin{pmatrix} \sigma_x \\ \sigma_y \\ \tau_{xy} \end{pmatrix}$$

To close the problem we need boundary conditions on the borders of our domain.

$$\boldsymbol{\sigma} \cdot n_t = \boldsymbol{\sigma}_H \quad \text{on} \quad \Gamma_L \cup \Gamma_R \tag{2.7a}$$

$$\boldsymbol{\sigma} \cdot n_t = \boldsymbol{\sigma}_h \quad \text{on} \quad \Gamma_T \cup \Gamma_B \tag{2.7b}$$

$$\boldsymbol{\sigma} \cdot n_f = p(s,t) \quad \text{on} \quad \Gamma_f \tag{2.7c}$$

$$u = 0 \quad \text{on the four vertices} \tag{2.7d}$$

2.1.3. ADVANCE CRITERION

The fracture propagation criterion that we have adopted is based on Griffith's theory, which is sustained on energy considerations around the crack tip. This criterion considers that the fracture propagates when the *Stress Intensity Factor* (K') equals the material parameter *Fracture Toughness* (K_C) in the crack tip (2.8). In fact what is used is not the *Fracture Toughness* but the *Effective Fracture Toughness* (K_C') because it is shown that the rock hardness measured in the lab is lower than the real one due to scale effect, to the influence of confining in-situ stress, to micro-cracking and to plasticity in the process zone near the crack-tip [2]:

$$\begin{cases} \dot{l} = 0, K' < K_C' \\ \dot{l} > 0, K' = K_C' \end{cases} \tag{2.8}$$

where $\dot{l}$ is the time derivative of the fracture length l. In our case the computation of K' is done with an integral approximation that accounts for both the solid displacement (I_u) and also for the nonzero tractions of the pressure (I_p) all along the fracture domain [20]:

$$K' = \frac{4}{\pi(1-\nu)} (I_u + I_p) \tag{2.9}$$

with the integral expressions for the displacement and pressure contributions:

$$I_u = \int_\Omega \left[\left(\boldsymbol{\sigma}_{im}^{\boldsymbol{\psi}} u_{i,j} + \boldsymbol{\sigma}_{im} \psi_{i,j} \right) e_j - \boldsymbol{\sigma}_{ij} \psi_{i,j} e_m \right] \chi_{,m} d\Omega \tag{2.10}$$

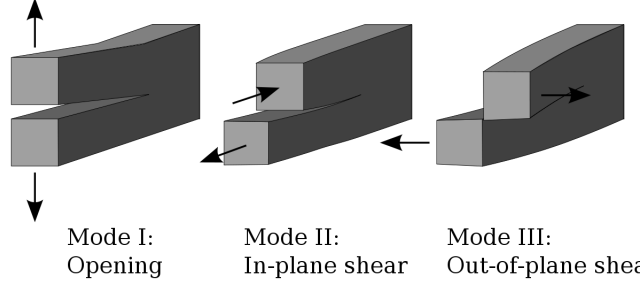$$I_f = \int_{\Gamma_p} (p\chi)_{,1} \psi_2 d\Gamma_f \tag{2.11}$$

Mode I: Mode II: Mode III:
Opening   In-plane shear   Out-of-plane shea

Figure 2.2: Scheme of the three different crack modes defined in fracture mechanics.

where $\boldsymbol{\sigma_{ij}}$ are the components of the stress tensor, and e is a unit vector tangential to the crack face and pointing out to the uncracked material.

In equations (2.10) and (2.11) the parameters ψ_1 and ψ_2 representing the Cartesian components of the auxiliary displacement field ψ undergoing pure tensile fracturing, Mode I (see Figure 2.2) are introduced:

$$\psi_1 = r^{1/2} \cos\left(\frac{\theta}{2}\right)(\kappa - \cos\theta) \tag{2.12}$$

$$\psi_2 = r^{1/2} \sin\left(\frac{\theta}{2}\right)(\kappa - \cos\theta) \tag{2.13}$$

with $\kappa = 3 - 4\nu$ in plane-strain and r is the distance to the crack tip. The corresponding stress field to ψ_1 and ψ_2 is:

$$\boldsymbol{\sigma_{ij}^{\psi}} = \mathbb{C}_{ijkl}\psi_{k,l} \tag{2.14}$$

where $\mathbb{C}$ is the fourth-order elastic constitutive tensor (2.5).

Since the *Stress Intensity Factor* affects only the proximities of the crack tip, in equations (2.10) and (2.11) the auxiliary scalar parameter χ has been introduced. This parameter in our case is defined as:

$$\chi = \begin{cases} 1 & \text{if} \quad r \leq r_\chi \\ 0 & \text{if} \quad r > r_\chi \end{cases} \tag{2.15}$$

where r_χ is a radius of interaction that in the discrete case is taken to be a few number of elements.

2.2. FEM FORMULATION

As we have explained, in this Master's Thesis we aim to prove the validity of two ROM's in the case of hydraulic fracturing problem: POD and PGD. For the POD we first need a set of *snapshots* of the solution to extract the relevant information and create the basis for the ROM. In our case we have chosen the Finite Element Method to solve the model and feed POD. For this purpose we need to define the weak forms of both fluid and solid problems and then couple both equations.

2.2.1. FLUID EQUATION WEAK FORM

To get the weak form of the Poiseuille's equation (2.1a), we define δp as the variations of p, multiply both sides of the equations, integrate over the fluid domain Ω_f and then use integration by parts in the term with second order derivatives.

$$\int_{\Omega_f} \delta p \frac{\partial w}{\partial t} d\Omega_f = \left[\delta p \frac{w^3}{12\mu} \frac{\partial p}{\partial s}\right]_{\Gamma_f} - \int_{\Omega_f} \frac{\partial \delta p}{\partial s} \frac{w^3}{12\mu} \nabla p d\Omega_f + \int_{\Omega_f} \delta p \delta(s) Q_0 d\Omega_f \tag{2.16a}$$

$$\left[\delta p \frac{w^3}{12\mu} \frac{\partial p}{\partial s}\right]_{\Gamma_f} = 0 \tag{2.16b}$$

The time derivative is replaced by a Finite Difference discretization:

$$\frac{\partial w}{\partial t} = \frac{w^{n+1} - w^n}{\Delta t} \tag{2.17}$$

Using a Finite Elements approximation we define:

$$p = \sum_{i=1}^{n_p} N_p^i \boldsymbol{p}_i \qquad\qquad u = \sum_{i=1}^{n_u} N_u^i \boldsymbol{u}_i \qquad\qquad w = A \sum_{i=1}^{n_u} N_u^i \boldsymbol{u}_i \tag{2.18}$$

where N^p and N^u are the 1D pressure and 2D solid shape functions, and $\boldsymbol{p}$ and $\boldsymbol{u}$ the vectors of components of pressure and displacement respectively. A is a geometrical rectangular matrix ($n_{fluid} \times 2n_{solid}$)that transforms the solid displacement into fracture opening.

With this discretization and using Galerkin method we define the matrix form of the problem as:

$$\frac{1}{\Delta t} M_f A \boldsymbol{u}^{n+1} + K_f \boldsymbol{p}^{n+1} = f_f \frac{1}{\Delta t} M_f A \boldsymbol{u^n} \tag{2.19a}$$

$$K_f = \int_{\Omega_f} (\nabla N_p)^T \frac{w^3}{12\mu} \nabla N_u d\Omega_f \tag{2.19b}$$

$$M_f = \int_{\Omega_f} (N_p)^T N_u d\Omega_f \tag{2.19c}$$

$$f_f = \int_{\Omega_f} (N_p)^T \delta Q_0 d\Omega_f \tag{2.19d}$$

where K_f is the stiffness matrix of the fluid problem, M_f is the mass matrix of the fluid problem and f_f is the force vector.

Note here that the stiffness matrix of the fluid problem (2.19b) is non-linear because we integrate the cubic fracture opening $\frac{w^3}{12\mu}$ that in addition is time dependent. Therefore this term will have to be integrated at each time step with the new value of fracture opening w in an iterative way till stabilization is reached.

2.2.2. SOLID EQUATIONS WEAK FORM

Now to obtain the weak form of the solid problem we define δu as the variations of u, multiply all terms and using the divergence Gauss theorem to the second order derivative term, we get:

$$\int_{\Omega_s} \nabla \delta u^T \boldsymbol{D} \nabla^s \boldsymbol{u} d\Omega - \int_{\Gamma_{out}} \delta u^T \boldsymbol{\sigma_0} d\Gamma - \int_{\Omega_f} \delta u^T \boldsymbol{p} d\Omega_f = 0 \tag{2.20}$$

Discretizing likewise equation (2.18) we obtain the matrix form of the solid problem:

$$K_s \boldsymbol{u}^{n+1} - M_s \boldsymbol{p}^{n+1} = f_s \tag{2.21a}$$

$$K_s = \int_{\Omega_s} \nabla (N_u)^T \boldsymbol{D} \nabla N d\Omega \tag{2.21b}$$

$$M_s = \int_{\Omega_f} (N_u)^T N_p d\Omega_f \tag{2.21c}$$

$$f_s = \int_{\Gamma_{out}} (N_u)^T \boldsymbol{\sigma_0} d\Gamma \tag{2.21d}$$

where K_s is the stiffness matrix of the solid problem, M_s is the mass matrix of the solid problem and f_s is the force vector.

Note here that unlike happened in the fluid formulation (2.19a), all matrices of the solid problem discrete form (2.21a) remain constant since they don't depend either in time nor in the fracture opening. Therefore we will only need to compute them once.

2.2.3. COUPLED PROBLEM

With the FEM formulations of both the fluid and the solid problem we express the matrix form of the coupled problem as:

$$\begin{bmatrix} K_s & -M_s \\ \frac{1}{\Delta t} M_f A & K_f \end{bmatrix} \begin{bmatrix} \boldsymbol{u}^{n+1} \\ \boldsymbol{p}^{n+1} \end{bmatrix} = \begin{bmatrix} f_s \\ f_f + \frac{1}{\Delta t} M_f A \boldsymbol{u}^n \end{bmatrix} \tag{2.22}$$

Solving this problem will mean inverting a matrix of order $(2n_{solid} + n_{fluid})^2$ terms at each time step, what even for small domains and coarse space discretization is an expensive process. To avoid this and taking advantage of the invariability of the solid matrices, we can invert only once the solid matrices.

$$\boldsymbol{u}^{n+1} = K_s^{-1} M_s \boldsymbol{p}^{n+1} + K_s^{-1} f_s = \boldsymbol{B} \cdot \boldsymbol{p}^{n+1} + \boldsymbol{b} \tag{2.23}$$

In this way we can write the fluid problem only in terms of pressure unknowns (2.24), solve for $\boldsymbol{p}^{n+1}$ and recover the solid displacements $\boldsymbol{u}^{n+1}$ as a post-process with (2.23).

$$\left[\frac{1}{\Delta t} M_f A \boldsymbol{B} + K_f \right] \boldsymbol{p}^{n+1} = f_f + \frac{1}{\Delta t} M_f A (\boldsymbol{u}^n - \boldsymbol{b}) \tag{2.24}$$

2.2.4. DOMAIN REDUCTION

Under the consideration of plane strain conditions and punctual injection source, the solution of the problem becomes symmetric with respect to both horizontal and vertical axes. Therefore a reduced domain of study of only a quarter of the fracture is adopted (Figure 2.3). After computing the solution in this reduced domain, it is possible to plot the hole domain just reflexing the solutions with the corresponding change in sign.
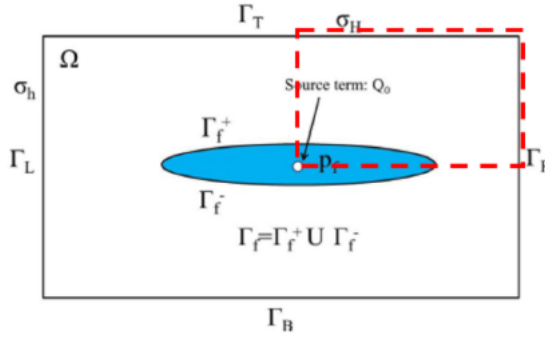

Figure 2.3: Sketch of the reduced domain. The red dashed line indicates the area of the reduced domain.

This domain reduction implies some special considerations in the formulation. The fracture opening w is twice the vertical displacement of the fracture solid nodes:

$$w = 2u_2 \quad \in \Gamma_f \tag{2.25}$$

therefore the geometrical matrix A that transforms vertical fracture displacements into fracture opening is defined as:

$$A_{ij} = \begin{cases} 2 \text{ if } i = n \quad \& \quad j = 2n \quad n \in \Gamma_f \subset X_s \\ 0 \text{ else} \end{cases} \tag{2.26}$$

Another modification in the formulation is in the boundary conditions. The perpendicular displacement of the solid nodes in the planes of symmetry is null.

$$u_1 = 0 \quad \in \Gamma_L \qquad\qquad\qquad u_2 = 0 \quad \in \Gamma_B \tag{2.27}$$

About the Neumann boundary conditions, the only change is that the prescribed tractions in the lower domain only affects the non-fractured domain.

$$\boldsymbol{\sigma} \cdot n_b = t_b \quad \in \Gamma_B \backslash \Gamma_f \tag{2.28}$$

Finally the inflow rate is half the prescribed one:

$$Q_{eff} = \frac{Q_0}{2} \tag{2.29}$$

2.3. PGD FORMULATION

In order to obtain a scheme that could be used to generate a PGD solution of our problem we need to reduce the coupled system to a single equation that expresses the fluid-solid interaction. This is done isolating the displacement unknown u^{n+1} from the matrix FE formulation 2.22 and replacing w in the fluid equation as a function of u which is also a function of p. In this way we get an equation where the only unknown is the pressure p.

In our formulation we want to find a space-time separable solution of the pressure so this pressure has to be rewritten as the sum of products of pairs of modes depending only on space and time respectively. In this way the new expression for the pressure is written as:

$$p_{PGD}^{m+1} = \sum_{i=1}^{m+1} X_i(x) T_i(t) = X^{m+1}(x) T^{m+1}(t) + \sum_{i=1}^{m} X_i(x) T_i(t) = X^{m+1}(x) T^{m+1}(t) + p_{PGD}^m \tag{2.30}$$

what makes possible to construct the new approximation p_{PGD}^{m+1} as a correction of the previous solution p_{PGD}^{m-1}.

Finally we are able to compute the displacement field and the fracture opening as a transformation of the pressure field:

$$u^{m+1} = K_s^{-1} M_s p^{m+1} + K_s^{-1} f_s = \boldsymbol{B} \cdot p^{m+1} + \boldsymbol{b} \tag{2.31}$$

$$w^{m+1} = A \cdot u^{m+1} = A(\boldsymbol{B} \cdot p^{m+1} + \boldsymbol{b}) \tag{2.32}$$

where A is a geometrical matrix that extracts the vertical component of the displacement of the fracture nodes (2.26).

The separable expression of the solution as the product of space and time modes allows the construction of the solution for all nodes and for all time. Therefore and since we have expressed the coupled system only in terms of pressure, the governing equation of the system is derived from the fluid weak form. This implies that the integrals of the weak form now are not only over space but also over time (2.33).

$$\int_{\Omega_f \times \Omega_t} \delta p \, \dot{w} \, dt \, d\Omega_f + \int_{\Omega_f \times \Omega_t} \nabla(\delta p) \frac{w^3}{12\mu} \nabla p \, dt \, d\Omega_f = \int_{\Omega_f \times \Omega_t} \delta p Q_0 \, dt \, d\Omega_f \tag{2.33}$$

Now to find the space and time modes we use an Alternating Direction Scheme (fixed-point solver). This consists in first solve for space modes X^{m+1} assuming time T^{m+1} known, and then solve for time T^{m+1} with the just-computed space mode X^{m+1} and iterate this process till the new computed modes stabilizes or a maximum of iterations.

Then the equation for finding the space mode X^{m+1} is obtained defining δp as the variations of p, namely $X^* T^{m+1}$ in (2.33).

$$\int_{\Omega_f \times \Omega_t} (X^* T^{m+1}) \dot{w} \, dt \, d\Omega_f + \int_{\Omega_f \times \Omega_t} \nabla(X^* T^{m+1}) \frac{w^3}{12\mu} \nabla p \, dt \, d\Omega_f = \int_{\Omega_f \times \Omega_t} (X^* T^{m+1}) Q_0 \, dt \, d\Omega_f \tag{2.34}$$

and the equation for finding the time mode T^{m+1} is obtained defining δp as the variations of p, namely $X^{m+1} T^*$ in (2.33).

$$\int_{\Omega_f \times \Omega_t} (X^{m+1} T^*) \dot{w} \, dt \, d\Omega_f + \int_{\Omega_f \times \Omega_t} \nabla(X^{m+1} T^*) \frac{w^3}{12\mu} \nabla p \, dt \, d\Omega_f = \int_{\Omega_f \times \Omega_t} (X^{m+1} T^*) Q_0 \, dt \, d\Omega_f \tag{2.35}$$

with

$$\dot{w} = AB\dot{p} = AB \left(X^{m+1} \dot{T}^{m+1} + \sum_{i}^{m} X^i \dot{T}^i \right) \tag{2.36}$$

Finally replacing terms and operating it leaves for the X^{m+1} mode:

$$\int_{\Omega_f}\left(X^*ABX^{m+1}\int_{\Omega_t}T^{m+1}\dot{T}^{m+1}dt\right)d\Omega_f + \int_{\Omega_f}\left(\nabla(X^*)\frac{w^3}{12\mu}\nabla(X^{m+1})\int_{\Omega_t}T^{m+1}T^{m+1}dt\right)d\Omega_f$$

$$= \int_{\Omega_f}\left(X^*Q_0\int_{\Omega_t}T^{m+1}dt\right)d\Omega_f - \overset{m}{\underset{i}{\sum}}\int_{\Omega_f}\left(X^*ABX^i\int_{\Omega_t}T^{m+1}\dot{T}^i dt\right)d\Omega_f \tag{2.37}$$

$$- \overset{m}{\underset{i}{\sum}}\int_{\Omega_f}\left(\nabla(X^*)\frac{w^3}{12\mu}\nabla(X^i)\int_{\Omega_t}T^{m+1}T^i dt\right)d\Omega_f$$

and for the T^{m+1} mode:

$$\int_{\Omega_t}\left(T^*\dot{T}^{m+1}\int_{\Omega_f}X^{m+1}ABX^{m+1}d\Omega_f\right)dt + \int_{\Omega_t}\left(T^*T^{m+1}\int_{\Omega_f}\nabla(X^{m+1})\frac{w^3}{12\mu}\nabla(X^{m+1})d\Omega_f\right)dt$$

$$= \int_{\Omega_t}\left(T^*Q_0\int_{\Omega_f}X^{m+1}d\Omega_f\right)dt - \overset{m}{\underset{i}{\sum}}\int_{\Omega_t}\left(T^*\dot{T}^i\int_{\Omega_f}X^{m+1}ABX^i d\Omega_f\right)dt \tag{2.38}$$

$$- \overset{m}{\underset{i}{\sum}}\int_{\Omega_t}\left(T^*T^i\int_{\Omega_f}\nabla(X^{m+1})\frac{w^3}{12\mu}\nabla(X^i)d\Omega_f\right)dt$$

To solve the time problem (2.38) we have to localize and return to the strong form (2.39) which is a first order Initial Value Problem that we solve with the Runge-Kutta fourth-order method (RK4):

$$\dot{T}^m\int_{\Omega_f}X^mABX^m d\Omega f + T^m\int_{\Omega_f}\nabla(X^m)\frac{w^3}{12\mu}\nabla(X^m)d\Omega_f = Q_T\int_{\Omega_f}X^mQ_X d\Omega_f$$

$$- \overset{m-1}{\underset{i}{\sum}}\dot{T}^i\int_{\Omega_f}X^mABX^i d\Omega_f - \overset{m-1}{\underset{i}{\sum}}T^i\int_{\Omega_f}\nabla(X^m)\frac{w^3}{12\mu}\nabla(X^i)d\Omega_f \tag{2.39}$$

The remaining equations (2.37) and (2.38) are still non-linear due to the cubic opening term $\frac{w^3}{12\mu}$ which also has to be linearized and separated. To linearize it there are two possibilities [17]:

1. **Newton's method**: consists in linearize the governing equation before applying PGD

2. **Picard's method**: where the non-linear term is evaluated from the previous enrichment step

In our case we chose the Picard's one.

To separate the cubic term $\frac{w^3}{12\mu}$ in modes depending only on space and modes depending only on time we use Singular Value Decomposition (SVD), so we end up with a decomposition:

$$svd\left(\frac{w^3}{12\mu}\right) = \theta(x)\cdot\alpha\cdot\phi(t)^T \approx \overset{L}{\underset{l}{\sum}}\theta^l(x)\alpha^l(\phi^l(t))^T \tag{2.40}$$

where θ has the space modes, α represents the amplitudes of the modes and ϕ expresses the time modes. In this way we have obtained a linearized and separable representation of $\frac{w^3}{12\mu}$.

The injection term Q_0 also has to be expressed as the product of a function depending only on space and a function depending only on time (2.41). These functions are basically the injection rate in the nodes inside the pipe and zero elsewhere for space and all ones for the time since we inject during all the time domain at the same rate.

$$\int_{\Omega_f}\int_{\Omega_t}Q_0 dt d\Omega_f = \int_{\Omega_f}Q_0 d\Omega_f\int_{\Omega_t}dt = Q_X Q_T \tag{2.41}$$

For the matrix formulation of the problem we define:

$$K_f = \sum_l K_f^l \qquad\qquad\qquad K_f^l(x) = \int_{\Omega_f}\nabla N\theta(x)(\nabla N)^T d\Omega_f$$

$$M_f = \sum_l M_f^l \qquad\qquad\qquad M_f^l(t) = \int_{\Omega_f}\varphi\phi(t)\varphi^T dt$$

$$C(t) = \int_{\Omega t}\varphi(\nabla\varphi)^T dt \qquad\qquad M(x) = \int_{\Omega_f}NN^T d\Omega_f$$

And finally the matrix expression for the alternating direction strategy ends being:

$$[T^m(MABC)T^m + \sum_l \alpha^l K_f^l T^m M_f^l T^m]X^{m+1} = X^m Q_X T^m Q_T$$

$$- \sum_i^m X^m(MAB)X^i T^m C T^i - \sum_i^m X^m(\alpha^i M T^m C T^m - \sum_l K_f^l T^m M_f^l T^i)X^i \tag{2.42}$$

$$X^{m+1}(MAB)X^{m+1}\dot{T}^{m+1} + \sum_l X^{m+1}K_f^l \phi^l X^{m+1} T^{m+1} =$$

$$X^{m+1}Q_X Q_T - \sum_i^m X^{m+1}(MAB)X^i \dot{T}^i - \sum_i^m \sum_l X^{m+1}K_f^l \phi^l X^i T^i \tag{2.43}$$

The alternating direction strategy defined by equations (2.42) and (2.43) is solved sequentially first for X^{m+1} with (2.42) and then for T^{m+1} with (2.43) and this process is iterated some times. The alternating direction scheme defined above finds modes in a sequential way, and then the procedure is iterated to ensure stability of the non-linear term. For the proper function of the alternating direction strategy it is necessary to normalize the first mode of the iterative solver, in our case the spatial mode X, to ensure that the amplitude of the solution is only counted in the second mode. This strategy requires of a proper initial pressure distribution to avoid negative pressures, the first mode is devoted to impose this initial pressure distribution. This is done likewise in FEM finding a proper initial pressure with equation (2.3).

The resulting alternating direction scheme is formed by equation (2.42) which is an algebraic equation that is solved with a proper linear system of equation solver.

On the other hand equation (2.43) is a first order ordinary differential equation that we solve with the fourth order Runge-Kutta method with an appropriate initial value. To use this method we have to define the expression for the time derivative $\dot{T}^{m+1}$:

$$F(T(t)) = \dot{T}^{m+1} = \frac{X^{m+1}Q_X Q_T - \sum_i^m X^{m+1}(MAB)X^i \dot{T}^i(t) - \sum_i^{m+1}\sum_l X^{m+1}K_f^i X^i \phi^l T^i(t)}{X^{m+1}(MAB)X^{m+1}} \tag{2.44}$$

For the time derivatives of the already computed modes $\dot{T}^i$ we use an explicit finite differences approach:

$$\dot{T}^i(n) = \frac{T^i(n) - T^i(n-1)}{\Delta t} \tag{2.45}$$

The Runge-Kutta fourth order method is defined as:

$$T(n+1) = T(n) + \frac{\Delta t}{6}(k_1 + 2k_2 + 2k_3 + k_4) \tag{2.46}$$

$$k_1 = F(t, T(n)) \qquad\qquad k_3 = F(t + \frac{\Delta t}{2}, T(n) + \frac{\Delta t}{2}k_2)$$

$$k_2 = F(t + \frac{\Delta t}{2}, T(n) + \frac{\Delta t}{2}k_1) \qquad\qquad k_4 = F(t + \Delta t, T(n) + \Delta t k_3)$$

which needs an initial condition T^0 to start the loop, in our case we have chosen $T^0 = 0$.

<div align="right">

3

</div>

NO FRACTURE ADVANCE

A first simplified model that accounts only for fracture inflation and not for propagation has been proposed to check the suitability of a Model Order Reduction. First the POD approach is shown and then also the PGD one.

3.1. MODEL PARAMETERS

For all the simulations of this simplified model with no fracture advance, the material parameters have been taken in the range of a potential *shale oil* reservoir [18] and are listed in Table 3.1. The far field stress σ_0 is those of around 1500 m depth, which is a normal depth for a reservoir of this kind.

Parameter	Symbol	Value	Unit
Young's modulus	E	14400	[MPa]
Poisson's ratio	ν	0.2	[-]
Fluid viscosity	μ	1×10^{-3}	[MPa $\cdot s$]
Far field stress	σ_0	27.7579	[MPa]

Table 3.1: Material parameters used in the simulation of hydraulic fracturing without crack advance [18].

The model numerical parameters used in the simulations are summarized in 3.2.

| Parameter	Symbol	Value	Unit
Inflow rate	Q_0	0.2	$[m^3/s]$
Pipe width	r	0.25	$[m]$
Initial fracture length	L_0	1	$[m]$
Time interval	t_{mesh}	$[0,1]$	$[s]$
Initial fracture opening	w_0^*	1×10^{-3}	$[m]$

Table 3.2: Model parameters

3.1.1. SPACE DISCRETIZATION

The spatial discretizations used to simulate the opening of a predefined hydraulic fracture consists in a 2D mesh of fourth noded $\mathbb{Q}_1$-quadrilaters to model the solid domain, with vertical and horizontal degrees of freedom, and a 1D two noded linear mesh for the fluid pressure.

To avoid that the solid boundary conditions affects the fracture Γ_f domain, the spatial discretization is fourth times longer than the fracture length $\Omega = [0,4] \times [0,2]$. To chose an appropriate mesh size, we have compared different meshes using the same time step of $\Delta t = 0.01$ to see its influence on the FEM solution. Concretely the injection node end time pressure has been compared for sequential finer meshes $h = [0.25, 0.125, 0.0625, 0.03125]$. It is seen in Figure 3.1a that as the mesh is refined, the pressure tends to

stabilize. Unfortunately we don't have access to more computational resources and we can't refine more the mesh to obtain more stability. Looking at the results, the mesh size adopted has been the finest possible $h = 0.03125$.
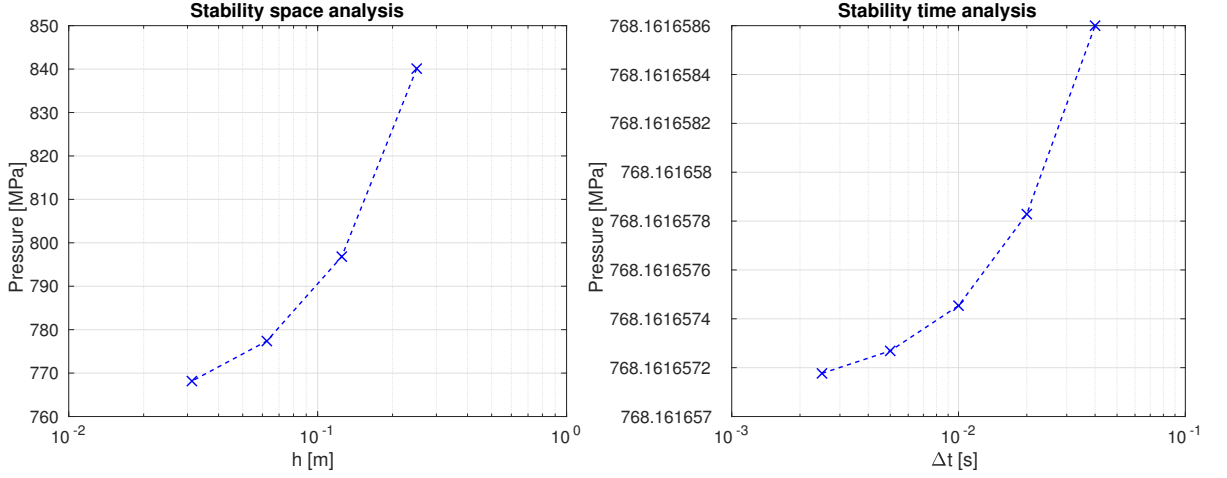
(a) Different space discretizations.

(b) Different time discretizations.

Figure 3.1: Stability analysis for both space and time discretizations. The final injection node pressures are compared.

3.1.2. TIME DISCRETIZATION

Also to define a proper time discretization, the final injection node pressure for sequentially doubling time step steps $\Delta t = [0.0025, 0.005, 0.01, 0.02, 0.04, 0.1]$ with the same spatial discretization of $h = 0.03125$ have been compared. In Figure 3.1b the different results are plotted, and it is seen that the problem is much less sensible to the time mesh than the space one. Since the final result is not significantly affected by the time step, we are free to choose the number of solutions we want. We have chosen to get the *snapshots* for the POD solution $\Delta t = 0.01$, what means 101 solutions to see if the model order reduction is efficient or not.

3.2. POD

For the computation of the reduced order model solution with POD we first need to find a series of FEM *snapshots* for different times of the pressure p^i and store them in a matrix per columns. These solutions are found with standard Finite Elements space discretization and with a time marching scheme, with the only particularity of solving a nonlinear system of equations iteratively at each time step.

The numerical simulation of this model has been done in a code debugged in MATLAB, which its main loops are summarized in Algorithm 1.

After this, using the MATLAB command *svd* applied to the set of *snapshots* of the pressure we get as a result three matrices representing per columns:

1. **U**: the space modes   2. **S**: the amplitudes   3. **V**: the time modes

With these three matrices it is possible to recover the pressure p_{POD} at any time step i in an *on-line* phase just multiplying

$$p_{POD}^i = U(:, 1:k) \cdot S(1:k, 1:k) \cdot V(i, 1:k)^T \tag{3.1}$$

where k stands for the number of modes that we want to use to reproduce our POD solution.

If we are also interested in recover the solid deformation u and the fracture opening w, if we have stored B, b and A, it is easy and fast to recover them in a post-process that with two vector-vector multiplications like in equations (2.31) and (2.32).

```
 1  define boundary and initial conditions ;
 2  compute M_fB = (1/Δt) M_f A**B**;
 3  for i = 2 : n_steps do
 4  │   u^i = u^{i-1} ;
 5  │   p^i = p^{i-1} ;
 6  │   w^i = w^{i-1} ;
 7  │   error = inf ;
 8  │   norm = TOL ;
 9  │   j = 1 ;
10  │   while error > norm·TOL  &  j < maxIter do
11  │  │   compute K_f from w^i;
12  │  │   **a** = M_fB + K_f;
13  │  │   **c** = f_f + M_fB · p^{i-1};
14  │  │   p^i = **a**^{-1}**c**;
15  │  │   u^i = **B**p^i + **b**;
16  │  │   w^i = Au^i;
17  │  │   Δp = |p^i - p^{i-1}|;
18  │  │   error = √(Δp^T · K_f · Δp);
19  │  │   norm = √((p^i)^T · K_f · p^i);
20  │  │   j = j + 1;
21  │   end
22  end
```

Algorithm 1: Summarized FEM no fracture advance algorithm.

3.2.1. EXAMPLE

An example of the POD model order reduction has been computed using the parameters of Tables 3.1 and 3.2, with a tolerance for the non-linear loop of the FEM algorithm to get the solutions for the *svd* of $TOL = 1 \times 10^{-5}$. The discretizations used are those of sections 3.1.1 and 3.1.2. To see the efficiency of the model order reduction we have plot the amplitudes of the modes, which are represented in the diagonal of the **S** matrix in Figure 3.2a.

In Figure 3.2a it is seen a clear exponential decay in the mode's amplitudes, which allows to recover the FEM solution with fewer modes than the total non zero 33 produced that correspond to the minimum size of the matrix of *snapshots*, in this case the spatial degrees of freedom. In this case it is shown that at the eleventh mode the amplitudes flatten at almost machinery precision, what means that all the rest of modes are superfluous. Actually in the presented example the first amplitude represent the 99.8974% of all the modes amplitudes, and together with the second mode represents the 99.9993%. This allows to recover the "exact" FEM solution instead of storing 3333 entries with only 270, this is 8.1008% of the storage, with a maximum relative difference of 0.0289%.

The fact that with so few elements we could recover the time evolution of the pressure fracture profile is a consequence of the special characteristics of the problem. In this case, since the pressure profile is almost constant inside the fracture and the time evolution linear due to the linear elastic solid model adopted, the solution at any time can be accurately recovered with low order modes. Therefore the model order reduction of the hydraulic fracturing problem without fracture advance is clearly proven to be effective for the case of POD.

As an example of the graphical representation of the orthogonal modes resulting from the *svd* of the pressure *snapshots*, the firsts five space and time POD modes are presented in Figures 3.3a and 3.3b. It is seen that each new space mode is of one order more than the previous one to capture better the response of the time evolution of the fracture pressure profiles.
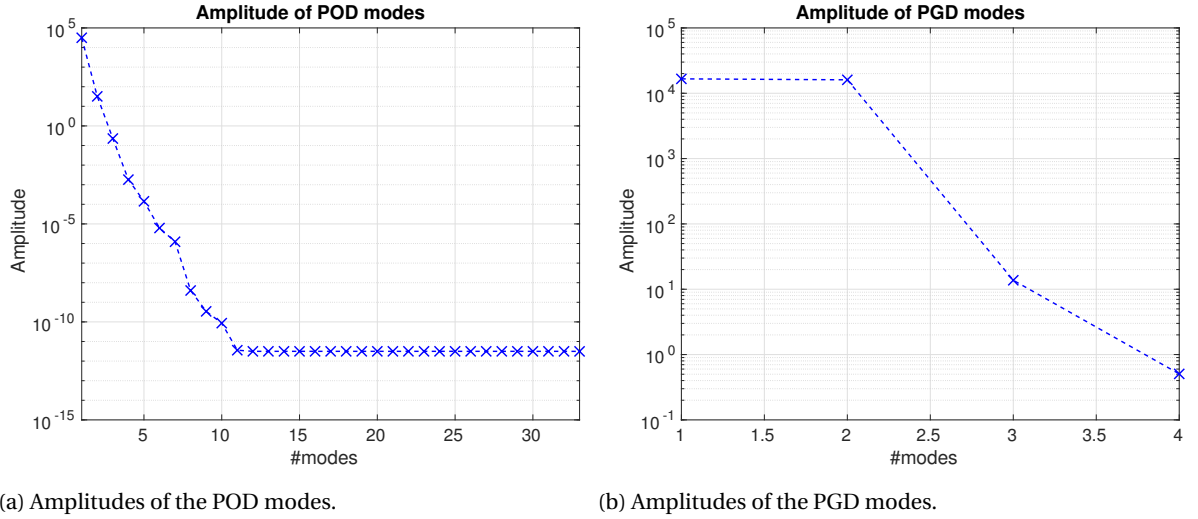
(a) Amplitudes of the POD modes.

(b) Amplitudes of the PGD modes.

Figure 3.2: Evolution of the mode's amplitudes for the POD and PGD reduced order models computed with discretizations $h = 0.03125\,m$ and $\Delta t = 0.1\,s$.

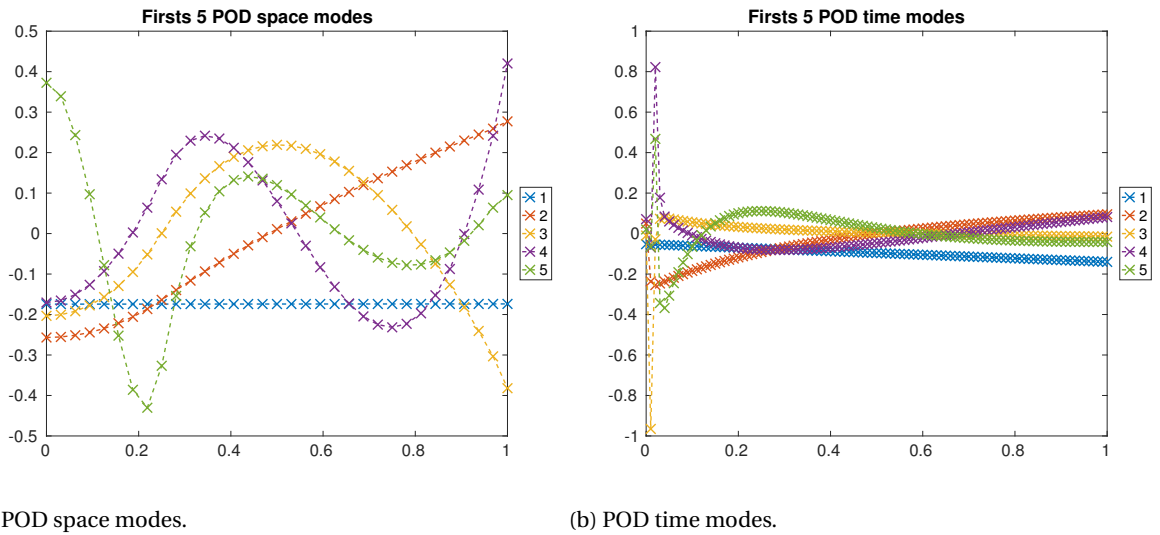(a) POD space modes.

(b) POD time modes.

Figure 3.3: Firsts five space and time modes resulting from the POD model order reduction of the hydraulic fracturing model without crack advance.

Finally in the post-process we can compute the displacement field from the pressures with (2.31) just with matrix-vector operations. Also it is possible to compute the components of the strain and stress tensors from the displacement field. In addition although our computational domain has been reduced to just one quarter, the solution can be extended to the original domain just assigning in the rest of three quarters the symmetric values of the reduced one. As an example of this, the end time fracture opening and vertical strain ϵ_{yy} have been plotted in Figure 3.4. We note that the effect of the fracture inflation on the crack tip is very local, and the deformation in most of the domain is almost zero. This makes interesting study the application of an adaptive mesh refining algorithm to catch the effect near the fracture while keeping a coarse mesh in the rest.
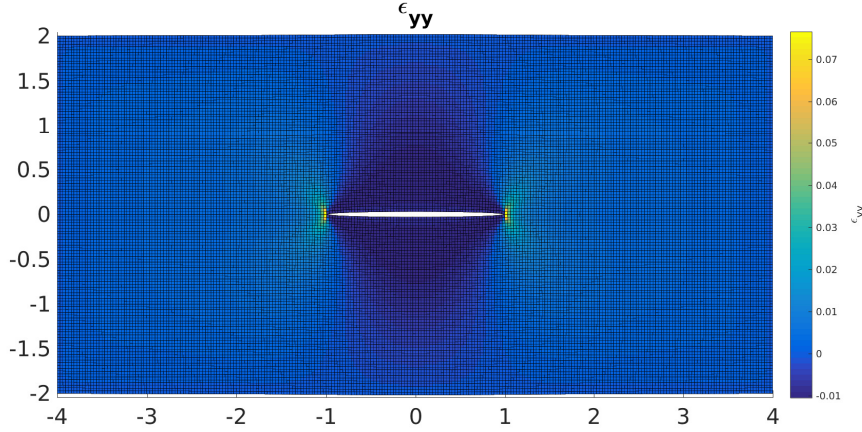
Figure 3.4: End time ($t = 1s$) fracture opening and vertical component of the strain ϵ_{yy} for the no fracture advance hydraulic fracturing model.

3.3. PGD

To apply the formulation of the PGD model order reduction a code has been developed in MATLAB, which is summarized in Algorithm 2. Before initializing the loops the firsts space and time modes are computed to accomplish with initial conditions. In this way the initial pressure is computed likewise in FEM with Equation (2.3). The space mode is assigned to be a normalized constant vector. The time mode is also assigned to be a constant vector with amplitude the computed initial pressure. The amplitude is assigned to the time mode and not to the space one because in the alternating direction strategy the space modes will be normalized while the time ones will have the amplitude.

The most external loop is a non-linear loop that updates the Singular Value Decomposition of the cubic opening term $\left(\frac{w^3}{12\mu}\right)$ with the updated PGD solution. The stopping criteria adopted for this process is based on stability of two successive iterative solutions (3.2):

$$max(p_{PGD}^i - p_{PGD}^{i-1}) < nonLinearTol \tag{3.2}$$

Inside this non-linear loop there is a second loop that controls the addition of new modes. This loop starts with the initialization of new modes in case in the previous non-linear iteration there was less modes. If we need to add new modes these are initialized with a vector of ones for both space X and time T. Since unlike in POD we don't have an *a priori* solution, our stopping criteria cannot be based on an error with respect to the precomputed solution. Instead of this we use a criteria based on the importance of the new computed mode with respect to the already computed separable solution p^{i-1}. The stopping criteria is therefore (3.3):

$$\frac{\|X^j T^j\|}{\|p_{PGD}^{j-1}\|} < tolPGD \tag{3.3}$$

This stopping criteria is sustained in the fact that, since we compute the $m - th$ PGD solution as an improve of the $m-1$ solution, the algorithm flats when the equation balance and no further improve is possible.

Finally the most internal loop is a fixed point iterative solver (alternating direction strategy) where the

---

1 initialize X^1 and T^1;
2 $i = 1$;
3 **while** $max(p_{PGD}^i - p_{PGD}^{i-1}) > nonLinearTol \ or \ i < maxNonLinearIter$) **do**
4   compute K_f and M_f of w_{PGD}^{i-1};
5 $j = 2$;
6   **while** $\|X^j T^j\|/\|p_{PGD}^{j-1}\| > tolPGD \ or \ j < maxModes$ **do**
7   **if** $j > modes(p_{PGD}^{i-1})$ **then**
8   initialize X^j and T^j;
9   compute K_f, M_f and ϕ of the $j - th$ mode;
10   **end**
11 $k = 1$;
12   **while** $\|X^k T^k - X^{k-1} T^{k-1}\| > alternateTol \ or \ k < maxIter$ **do**
13   compute X^{k+1} from T^k;
14   compute T^{k+1} from X^{k+1};
15 $k = k + 1$;
16   **end**
17 $j = j + 1$;
18   **end**
19 $i = i + 1$;
20 **end**

Algorithm 2: Summarized PGD no fracture advance algorithm.

---

stopping criteria is:

$$\|X^k T^k - X^{k-1} T^{k-1}\| < alternateTol \tag{3.4}$$

3.3.1. EXAMPLE

An example of the efficiency of the PGD reduced order model is presented here with the material parameters of 3.1 and the algorithm tolerances of Table 3.2 and the discretizations described in sections 3.1.1 and 3.1.2.

Parameter	Value
$nonLinearTol$	1×10^{-3}
$alternateTol$	1×10^{-2}
$tolPGD$	1×10^{-3}

Table 3.3: Tolerances of the PGD algorithm.

In this example our algorithm stopped at four modes and their amplitudes are plotted in Figure 3.2b. As seen the two firsts mode's amplitudes are of the same order because the first mode is devoted to impose the initial condition and the rest to reconstruct the solution. The first space mode corresponds to the pressure profile resulting of the solution of (2.3), a profile that we have assigned in all the time intervals through a constant unitary time mode. The shape of these firsts and rest of modes are plotted in Figure 3.5a and 3.5b.

Unlike what happened in the case of POD, in this case the resulting space modes (Figure 3.5a) aren't successively of one order more, but corrections to the first mode shape. This is a consequence of the construction of the PGD solution as an improve of the previous solution, then since we have explained in the case of POD the pressure profile is almost constant and we already assign a proper initial condition, the new PGD space modes just adjust the previous ones.

To see the "accuracy" of the PGD solution, since we don't have an analytical solution and just to see if the solutions produced are consistent with the ones computed with FEM, we have computed the relative difference of the FEM and PGD solutions as:
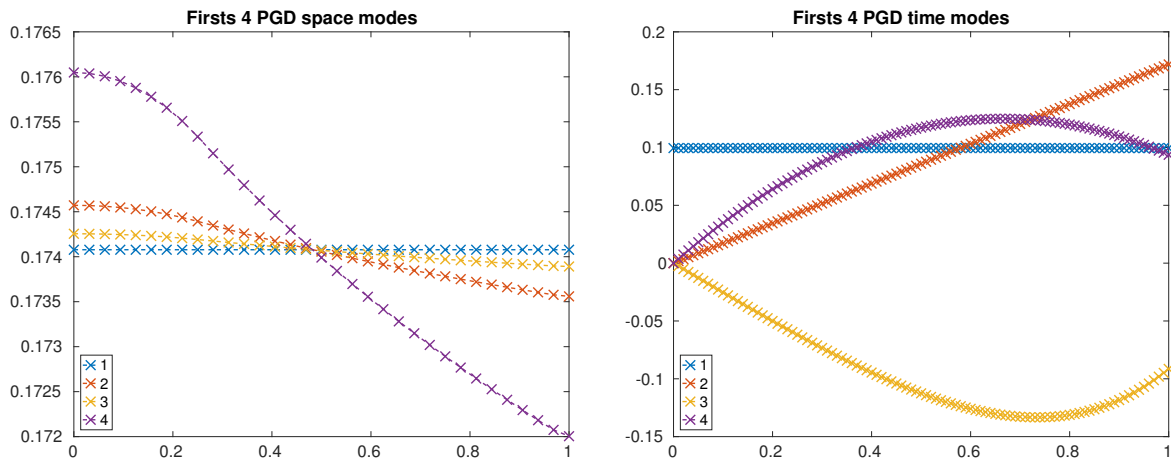
(a) PGD space modes.   (b) PGD time modes.

Figure 3.5: Space and time modes resulting from the PGD model order reduction of the hydraulic fracturing model without crack advance.

$$p_{diff}[\%] = \frac{100 \cdot |p_{FEM} - p_{PGD}|}{p_{FEM}} \tag{3.5}$$

The time evolution of this relative difference is plotted in Figure 3.6. It is seen that the maximum FEM-PGD difference is of only 1.0722%. As we have admitted this is not a measure of the error, but this is enough for us to ensure that the separability formulation proposed and the algorithm used produce similar solutions to FEM and therefore, likewise happened in POD, the model order reduction of the hydraulic fracturing problem without crack advance is possible.
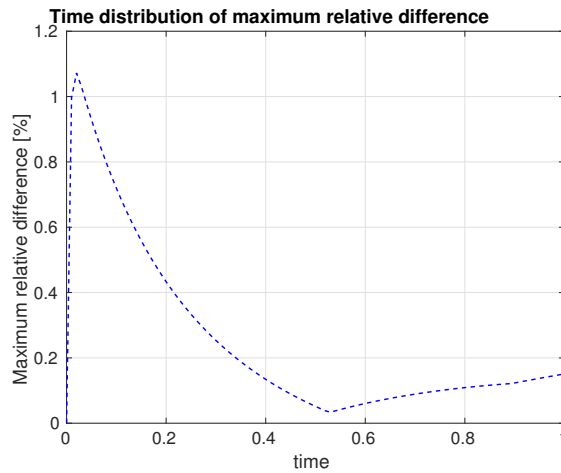

Figure 3.6: Time evolution of maximum relative PGD differences with 4 modes.

<div style="text-align: right; font-size: 3em; font-weight: bold;">4</div>

FRACTURE ADVANCE

After proving the validity of a Model Order Reduction for both POD and PGD for the hydraulic fracturing problem of a predefined fracture, now we want to study if it is possible to do the same with a fracture that do advances.

4.1. MODEL PARAMETERS

In this case for the simulations of the fracture advance and to avoid numerical instabilities the model parameters have been Table 4.1:

Parameter	Symbol	Value	Units
Inflow rate	Q_0	20	$[m^3/s]$
Pipe width	r	0.25	$[m]$
Initial fracture length	L_0	$16h = 0.5$	[m]
Initial fracture opening	w_0^*	1×10^{-3}	$[m]$
Fracture toughness	K_C'	5×10^3	[MPa·$\sqrt{m}$]
Number of time steps	n_{steps}	24	[-]
Interaction radius	r_χ	$2h = 0.0625$	[m]

Table 4.1: Model parameters of the hydraulic fracturing problem with fracture advance.

4.2. POD

To find a set of *snapshots* of the hydraulic driven fracture advance to then apply *svd*, first we solve the problem with FEM. Unlike what happened in the case of no fracture advance where we prescribed the fracture length, now the length will change so we need a different approach. If our objective was to capture the trajectory of the tip and the fracture opening, the best approach would be an Arbitrary Lagrangian-Eulerian (ALE) formulation with moving nodes in the crack tip. In this way we could enforce that a node always coincides with the tip.

However a changing mesh is not possible in our case because to be able to reproduce the solution with POD, all the *snapshots* must be taken with the same spatial mesh. Therefore we need an approach that could capture the fracture advance with a constant spatial discretization.

The advancing criterion (2.8) is such that the fracture grows when the *Stress Intensity Factor* (K') equals the *Fracture Toughness* (K_C'). In a discrete model with fixed mesh the fracture grows element by element, so we have applied a code able to capture the exact time instant when the new fracture tip node reaches the *Fracture Toughness* (K_C').

This code applies a root finding algorithm (Bisection method) to find the time instant when the crack tip node reaches breaking conditions (Algorithm 3). This is done sequentially for each new node added to the

<div style="text-align: center;">25</div>

fracture iteratively changing Δt till their condition becomes $K' = K'_C$.

---

1 define boundary and initial conditions ;
2 j=1 ;
3 **for** $i = 2 : n_{frac\_nodes}$ **do**
4   define initial guesses Δt_1 and Δt_2 such that $(K'(\Delta t_1) - K'_C) < 0$ and $(K'(\Delta t_2) - K'_C) > 0$;
5   **while** $|K'(\Delta t_1) - K'(At_2)| > TOL$ & $j < maxIter$ **do**
6 $\Delta t_{new} = \frac{\Delta t_1 + \Delta t_2}{2}$;
7 $M_{fB} = \frac{1}{\Delta t} M_f A\mathbf{B}$;
8 $error = \inf$;
9 $norm = TOL$;
10 $k = 1$;
11   **while** $error > norm \cdot TOL$ & $k < maxIter$ **do**
12   compute K_f from w^k;
13 $\mathbf{a} = M_{fB} + K_f$;
14 $\mathbf{c} = f_f + M_{fB} \cdot p^{k-1}$;
15 $p^k = \mathbf{a}^{-1}\mathbf{c}$;
16 $u^k = \mathbf{B}p^k + \mathbf{b}$;
17 $w^k = Au^k$;
18 $\Delta p = |p^k - p^{k-1}|$;
19 $error = \sqrt{\Delta p^T \cdot K_f \cdot \Delta p}$;
20 $norm = \sqrt{(p^k)^T \cdot K_f \cdot p^k}$;
21 $k = k + 1$;
22   **end**
23   **if** $\left(K'(\Delta t_{new}) - K'_C\right) \cdot K'(\Delta t_1) > 0$ **then**
24 $\Delta t_2 = \Delta t_{new}$
25   **else**
26 $\Delta t_1 = \Delta t_{new}$
27   **end**
28 $j = j + 1$
29   **end**
30 $i = i + 1$;
31 **end**

Algorithm 3: Summarized FEM fracture advance algorithm.

4.2.1. EXAMPLE

An example of the efficiency of the POD model order reduction of the hydraulic fracturing problem with fracture advance is presented below with the material parameters of Table 3.1, space discretization of section 3.1.1 and fracture advance parameters of Table 4.1.

In Figure 4.1a the amplitudes of the POD modes are plotted. It is seen that for the case of not normalized space modes, the decrease in the mode's amplitudes is not as fast as it was in the case of no fracture advance. This implies that to interpolate the solution with good precision all modes are necessary and there is no possible model order reduction as it is seen in the comparison with the FEM solution (Figure 4.1b) computed with (3.5). This is due to the fact that the set of *snapshots* computed with FEM is of the form of equation (4.1), this is in each new time step we have a new no null pressure node.

$$p_{FEM} = \begin{pmatrix} p_{11} & p_{12} & \cdots & p_{1n_{steps}} \\ 0 & p_{22} & \cdots & p_{2n_{steps}} \\ \vdots & 0 & \cdots & p_{3n_{steps}} \\ \vdots & \vdots & \cdots & \vdots \\ 0 & 0 & \cdots & p_{mn_{steps}} \end{pmatrix} \tag{4.1}$$

Therefore the space modes (Figure 4.2a) resulting from the *svd* has to interpolate a new not null node at each step. The only way to do so is adding a new mode for each new fracture node. This makes this approach not reducible.
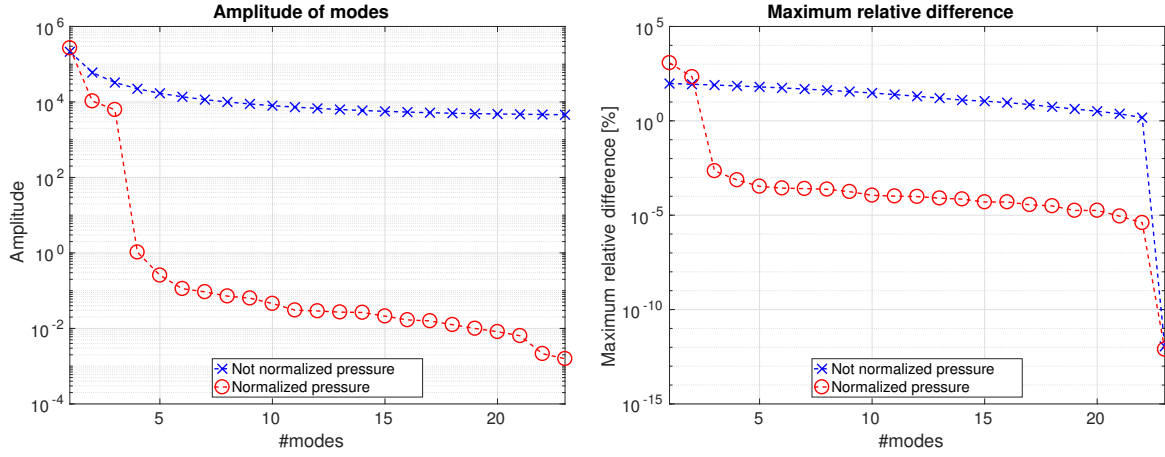
(a) Amplitudes.   (b) Maximum relative difference.

Figure 4.1: Comparison of the evolution of POD modes' amplitudes and maximum relative difference with FEM for not normalized and normalized pressures.

To check if it is possible to solve this problem with the space POD modes, we have interpolated the pressure *snapshots* with (4.2) to be all of the number of elements of the final fracture length in a normalized fracture domain $\hat{X} \in \hat{\Gamma}_f = [0, 1]$.

$$\hat{p}_{ij} = p_j^{up} + \frac{p_j^{up} - p_j^{low}}{\Delta X} \left(\hat{X}_i - \hat{X}_{i-1} \right) \tag{4.2}$$

This gives as a result a new set of *snapshots* of the form (4.3).

$$\hat{p}_{FEM} = \begin{pmatrix} \hat{p}_{11} & \hat{p}_{12} & \cdots & p_{1n_{steps}} \\ \hat{p}_{21} & \hat{p}_{22} & \cdots & p_{2n_{steps}} \\ \hat{p}_{31} & \hat{p}_{32} & \cdots & p_{3n_{steps}} \\ \vdots & \vdots & \cdots & \vdots \\ \hat{p}_{m1} & \hat{p}_{m2} & \cdots & p_{mn_{steps}} \end{pmatrix} \tag{4.3}$$

Then applying Singular Value Decomposition to this new set of solutions we obtain the POD modes and amplitudes. The first pressure solution of the FEM solution hasn't been used as a *snapshot* for the *svd* because doesn't correspond to a case of $K' = K'_C$. The result show a clear improve in the decay of modes amplitudes (Figure 4.1a) and maximum relative difference (Figure 4.1b). Although the amplitudes doesn't flatten at machine precision as happened in the case of no fracture advance, this normalization allows a model order reduction since the firsts 3 modes encloses the 99.9993% of the total amplitudes and is able to reproduce the solution with a maximum punctual relative difference with respect to FEM of only 0.0022%.

The change in the reducible character of the model between the not-normalized and normalized fracture domain is a consequence of not having to interpolate different fracture lengths. This change can be seen

comparing the firsts space modes for both the not normalized (Figure 4.2b) and normalized pressures (Figure 4.2a). The set of firsts fourth space modes of the normalized fracture domain (Figure 4.2b) are of similar shape, this means that many modes repeat most of the information contained in the firsts ones. This is a clear difference to the not-normalized spatial domain modes (Figure 4.2a) where the shape of modes is very different between them, so new information is not contained in the previous ones.
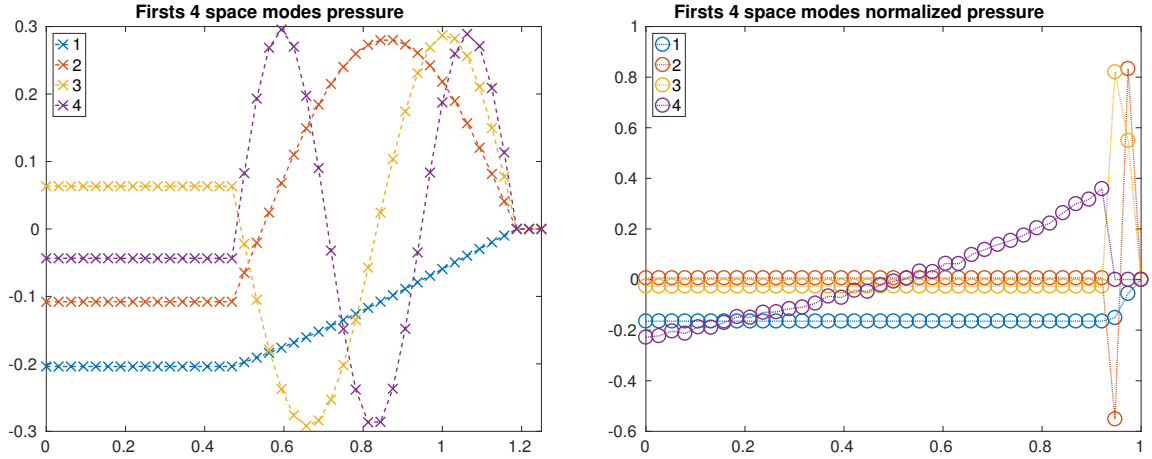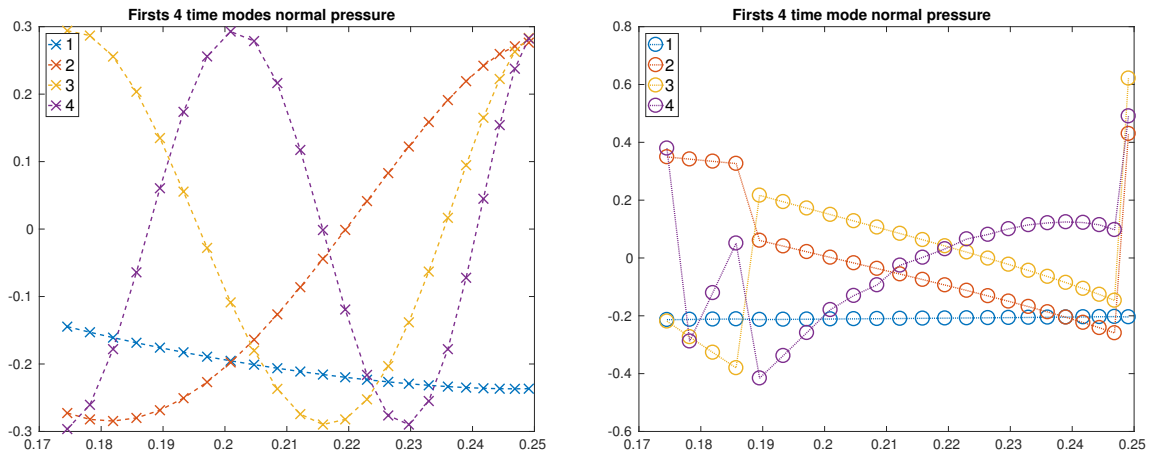

(a) Not normalized pressures   (b) Normalized pressures

Figure 4.2: Firsts 4 POD space modes for both not-normalized and normalized pressure *snapshots*.

For the case of the time modes (Figures 4.3a and 4.3b) they don't start at $t = 0s$ because as we have explained the initial time solution hasn't been used for the *svd* since wasn't a situation of $K' = K'_C$. Also unlike what happened in the case of no fracture advance these time modes doesn't have a constant time step Δt because the algorithm founds the time corresponding to $K' = K'_C$. However for the assumption of linear elastic solid the same crack elongation is found for similar time steps. What we do seen is that the more the fracture advances and the more it inflates, the faster reaches the *fracture toughness*.

(a) Not-normalized pressures   (b) Normalized pressures

Figure 4.3: Firsts 4 POD time modes for both not-normalized and normalized pressure *snapshots*.

Finally to see the graphical representation of the computational domain deformation we have plotted the end time fracture opening and vertical component of the strain likewise in the case of no crack advance

taking advantage of the symmetries of the problem in Figure 4.4. It is seen that for the material and model parameters adopted has to inflate a lot the fracture to reach the *fracture toughness*. The highest deformation is extension near the crack tips. This supports the assumption done for the case of fracture advance that the fracture advances radially to the fluid source due to mainly pure Mode I fracture since the in-plane shear strain corresponding to Mode II is negligible.
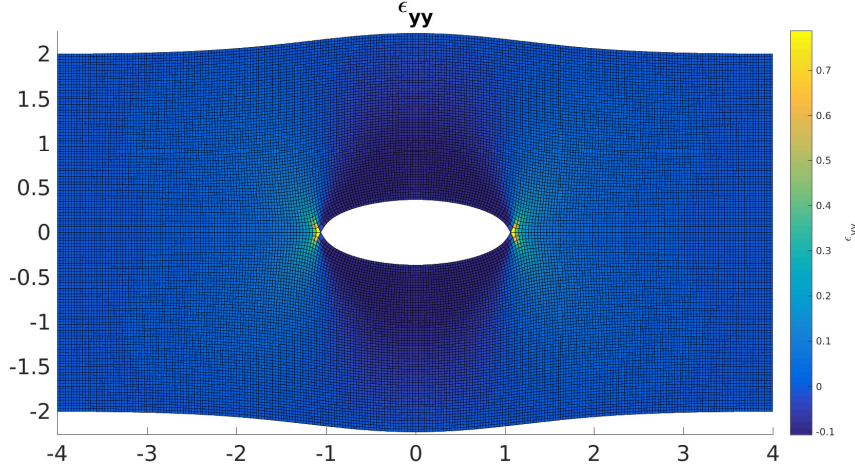

Figure 4.4: End time ($t = 0.2491 s$) fracture opening and vertical component of the strain ϵ_{yy} for the fracture advance hydraulic fracturing model.

4.3. PGD

As we have shown the hydraulic fracturing problem with fracture advance is not reducible in the case of different number of fracture elements. Then we have dismissed to code a PGD algorithm to find a separable representation of the pressure profile of the form (4.4).

$$p_{PGD} = \sum_i X_i(x) T_i(t) \qquad (4.4)$$

because there will not allow a model order reduction that is the objective of this master's thesis.

However we propose a possible future line of study that we haven't developed yet to achieve a model order reduction of the hydraulic fracturing problem with fracture advance with PGD.

4.3.1. FUTURE WORK

The analysis of the normalized pressure that we have done in the case of POD shows a descent in the amplitudes and difference with FEM, and makes possible think in a model order reduction also in the case of PGD. A possible way to obtain a model order reduction with PGD would be to introduce the fracture length l as a new variable in the separable expression of the pressure (4.5):

$$p_{PGD} = \sum_i \hat{X}_i(x) T_i(t) L_i(l) \qquad (4.5)$$

In this way it would be possible to have a set of spatial modes $\hat{X}$ that reproduce the inflation of the fracture of normalized length, a set of length modes L that could track the evolution of it and the time evolution with the time modes T.

5

CONCLUSIONS

In this thesis we have checked the feasibility of Reduced Order Models (ROM) applied to the hydraulic fracturing problem. First a simplified model of fracture inflation with no fracture advance has been proven for two reduced order methods: Proper Order Decomposition (POD) and Proper Generalized Decomposition (PGD).

In the case of POD since is an *a posteriori* ROM first a set of *snapshots* of the time evolution of the pressure inside the fracture is found with FEM. This solutions are then decomposed in three matrices using Singular Value Decomposition that represent space modes, time modes and amplitudes. The mode's amplitudes decrease as function of the reducible character of the problem solved. In the example presented the firsts 2 modes of a total of 33 encloses the 99.9993% of the total amplitudes. This allows to recover the FEM solution with a maximum difference of 0.0289% with a save in memory of around 90%, so the model order reduction with POD is proven.

On the other hand PGD is an *a priori* ROM so the solution is found directly. This property allow this method to be used apart of as a ROM as an efficient solver. A space-time separable expression of the fracture pressure has been proposed and in the example checked it has been proven to produce a reduced basis that with only 4 modes achieves a solution that doesn't differ of the FEM more than 1.0722%. So also with PGD it is possible to get a model order reduction of this problem.

A second model that accounts for fracture opening and lengthen has also been checked. The propagation criterion is based on the *Stress Intensity Factor* around the crack tip. The algorithm developed uses a fixed space mesh and a root finding strategy to capture the instant when the *Stress Intensity Factor* at the crack tip node equals the *Fracture Toughness*. In this case the set of *snapshots* for POD has a special shape since the pressure in all inactive fracture nodes are zero. This force the POD modes to interpolate in each time step a new not null element, what is only possible adding an extra mode. Therefore this approach is not reducible and the PGD case hasn't been developed.

To achieve a set of *snapshots* susceptible to be reduced in POD it is necessary to interpolate the pressures in the fracture to be all of the same number of elements. Doing this the reduction is possible and in the example presented with only 3 modes the FEM solution is recovered with a maximum relative difference of 0.0022%. This is why we propose this same approach to obtain the PGD separable expression, introducing a part of space and time, the fracture length as a new variable. We haven't develop this strategy yet and is proposed as a possible future line of study.

BIBLIOGRAPHY

[1] R. J. Clifton, A. S. Abou-Sayed, *et al.*, *A variational approach to the prediction of the three-dimensional geometry of hydraulic fractures,* in *SPE/DOE Low Permeability Gas Reservoirs Symposium* (Society of Petroleum Engineers, 1981).

[2] P. Papanastasiou, *The effective fracture toughness in hydraulic fracturing,* International Journal of Fracture **96**, 127 (1999).

[3] J. Walley, P. Aldous, *et al.*, *Environmental risks of fracking,* Tech. Rep. (UK's House of Commons).

[4] J. Adachi, E. Siebrits, A. Peirce, and J. Desroches, *Computer simulation of hydraulic fractures,* International Journal of Rock Mechanics and Mining Sciences **44**, 739 (2007).

[5] D. Van Dam, C. De Pater, and R. Romijn, *Experimental study of the impact of plastic rock deformation on hydraulic fracture geometry,* in *International Journal of Rock Mechanics and Mining Sciences and Geomechanics Abstracts,* Vol. 3 (1997) p. 439.

[6] R. Nordgren *et al.*, *Propagation of a vertical hydraulic fracture,* Society of Petroleum Engineers Journal **12**, 306 (1972).

[7] J. Geertsma, F. De Klerk, *et al.*, *A rapid method of predicting width and extent of hydraulically induced fractures,* Journal of Petroleum Technology **21**, 1 (1969).

[8] I. Sneddon, *The distribution of stress in the neighbourhood of a crack in an elastic solid,* in *Proceedings of the Royal Society of London A: Mathematical, Physical and Engineering Sciences,* Vol. 187 (The Royal Society, 1946) pp. 229–260.

[9] W. Schilders, *Introduction to model order reduction,* Model order reduction: theory, research aspects and applications , 3 (2008).

[10] P. Feldmann and R. W. Freund, *Efficient linear circuit analysis by padé approximation via the lanczos process,* IEEE Transactions on Computer-Aided Design of Integrated Circuits and Systems **14**, 639 (1995).

[11] A. Ammar, B. Mokdad, F. Chinesta, and R. Keunings, *A new family of solvers for some classes of multidimensional partial differential equations encountered in kinetic theory modeling of complex fluids,* Journal of Non-Newtonian Fluid Mechanics **139**, 153 (2006).

[12] A. Ammar, B. Mokdad, F. Chinesta, and R. Keunings, *A new family of solvers for some classes of multidimensional partial differential equations encountered in kinetic theory modelling of complex fluids: Part ii: Transient simulation using space-time separated representations,* Journal of Non-Newtonian Fluid Mechanics **144**, 98 (2007).

[13] S. Volkwein, *Proper orthogonal decomposition: Theory and reduced-order modelling,* Lecture Notes, University of Konstanz **4** (2013).

[14] L. De Lathauwer, B. De Moor, and J. Vandewalle, *A multilinear singular value decomposition,* SIAM Journal on Matrix Analysis and Applications **21**, 1253 (2000).

[15] S. Zlotnik, P. Díez, D. Modesto, and A. Huerta, *Proper generalized decomposition of a geometrically parametrized heat problem with geophysical applications,* International Journal for Numerical Methods in Engineering **103**, 737 (2015).

[16] E. Keogh and A. Mueen, *Curse of dimensionality,* in *Encyclopedia of Machine Learning* (Springer, 2011) pp. 257–258.

[17] F. Chinesta, R. Keunings, and A. Leygue, *The proper generalized decomposition for advanced numerical simulations : a primer,* p. 117.

[18] C. H. Yew and X. Weng, *Mechanics of hydraulic fracturing* (Gulf Professional Publishing, 2014).

[19] J. M. L. Poiseuille, *Experimental investigations on the flow of liquids in tubes of very small diameter,* Rheological Memoirs (1940).

[20] M. J. Hunsweck, Y. Shen, and A. J. Lew, *A finite element approach to the simulation of hydraulic fractures with lag,* International Journal for Numerical and Analytical Methods in Geomechanics **37**, 993 (2013).